



Repositorio Institucional de la Universidad Autónoma de Madrid

<https://repositorio.uam.es>

Esta es la **versión de autor** del artículo publicado en:

This is an **author produced version** of a paper published in:

ACS Applied Materials and Interfaces 8.22 (2016): 13934-13945

DOI: <http://dx.doi.org/10.1021/acsami.6b03081>

Copyright: © 2016 American Chemical Society.

El acceso a la versión del editor puede requerir la suscripción del recurso

Access to the published version may require subscription

Surface CuO, Bi₂O₃, and CeO₂ species supported in TiO₂-anatase: Study of Interface Effects in Toluene Photodegradation Quantum Efficiency

Mario J. Muñoz-Batista,¹ Anna Kubacka,^{1,*} Olga Fontelles-Carceller,¹ David Tudela,²
and Marcos Fernández-García^{1,*}

1 Instituto de Catálisis y Petroleoquímica. CSIC. C/ Marie Curie, 2. 28049 Madrid,
Spain

2 Departamento de Química Inorgánica, Facultad de Ciencias, Universidad Autónoma
de Madrid, Campus Cantoblanco, 28049 Madrid, Spain

Abstract

The enhancement of active triggered by surface deposition of Cu, Bi and Ce containing oxidic species onto a high surface area anatase is analyzed through the calculation of the quantum efficiency for toluene photo-degradation under UV and Sunlight-type illumination. To this end, series of Cu, Bi and Ce containing oxides supported onto anatase were synthesized having growing content of the Cu, Bi and Ce surface species and characterized with X-ray diffraction and photoelectron, UV-visible and photoluminescence spectroscopies as well as transmission electron microscopy. Utilizing the surface concentration of Cu, Bi and Ce species as a tool, we analyzed the influence of the system physico-chemical properties affecting quantum efficiency in anatase-based materials. First, employing small surface concentrations of the Cu, Bi and Ce species deposited onto (the unperturbed) anatase we provided evidence that all steps of the photocatalytic event, including light absorption, charge recombination as well as surface interaction with the pollutant and chemical output as to activity and selectivity have significance in the quantitative assessment of the enhancement of the efficiency parameter. Second, we analyzed samples rendering maximum quantum efficiency within all these series of materials. The study indicates that maximum enhancement over anatase displays a magnitude strongly dependent of the efficiency level of calculation and would thus require the use of the most accurate one, and that it occurs through a balance between optoelectronic and chemical properties of the composite materials. The (Cu,Bi,Ce) oxide-anatase interface plays a major role modulating the optoelectronic properties of the solids and thus the efficiency observable.

KEYWORDS: Anatase, Titania, Degradation; Quantum Efficiency and Yield; UV;
Sunlight; Oxide-Oxide interface

Corresponding author address: A.K. (ak@icp.csic.es), M.F.-G. (mfg@icp.csic.es)

1. Introduction

TiO₂ and particularly the anatase polymorph has been the subject to a wealth of research within the photocatalytic field. The highly activity of the anatase semiconductor material in almost all photo-degradation or photo-transformation reactions of organic and inorganic molecules and pollutants has been shown in many publications and has been summarized in review articles. In spite of it, more active materials are always sought and, particularly, the development of efficient catalysts for UV and visible wavelength lights simultaneously appears of primer importance in order to allow the fruitful use of solar light as a green energy source in photocatalytic processes.¹⁻⁵

An enhanced performance of anatase under UV and visible light has been pursued within a variety of approaches. Among the most successful ways, we can highlight the use of surface sensitizers consisting on semiconductor oxides with significant absorption capability in the visible range.^{2,5} Here we will consider the oxides of copper,⁶⁻¹⁷ bismuth,¹⁸⁻³⁰ and ceria³¹⁻⁴⁶ as they have been thoroughly tested in many photoreactions related to chemical pollutants or even biological entities degradation as well as in photoproduction of fuels or high value chemicals. Using these composite materials with anatase as common factor, we wish to analyze how the Cu, Bi and Ce-containing oxides can enhance photoactivity under UV and visible and, more importantly, sunlight illumination conditions.

The study of the photocatalytic behavior in quantitative basis requires the calculation and analysis of the efficiency parameter. According to the IUPAC definition, the calculation of the efficiency must take into account the number of molecules photo-transformed per photon absorbed at the catalytic material.⁴⁷ As described in recent works, this requires the accurate measurement of the catalytic surface illuminated and

thus catalytically active under illumination, the light handling properties of the whole (reactor+catalyst) system to calculate the net radiation flow at the catalyst' surface, as well as the catalytic properties including both activity and selectivity to obtain the number of reacting molecules as well as the number of charge species (and in turn photons) involved in the reaction.^{3,48-53} The whole procedure demands thus for a careful physico-chemical characterization of the materials as well as the careful analysis of their photochemical response under illumination conditions.

In this contribution we will attempt to carry out such study in these three CuO-TiO₂, CeO₂-TiO₂, and Bi₂O₃-TiO₂ systems as a function of the surface sensitizer concentration. In the low loading region we would like to estimate how a relatively minor disturbance of anatase would lead to significant enhancement of the photocatalytic performance and how this relates to the main light-matter and chemical properties involved in the quantum efficiency observable. Such study attempts to unveil the important physico-chemical properties of the anatase which are modified by interface interaction with surface ad-species and are critical for catalyzing the reaction. Moreover, special attention is paid to the comparative study of the activity maximum for the three composite sample series. A key question is how the activity is maximized when properly accounted by the quantum efficiency and what would be the specific physico-chemical characteristics through a sample series which trigger optimum response for the system (sample plus light characteristics) as a whole leading to maximum activity at the different illumination conditions tested in this work, i.e. UV, visible and sunlight. To this end, here we present the full analysis of the quantum yield as a function of its main light-matter and chemical variables and attempt to correlate the results with a multitechnique characterization approach using X-ray diffraction and

photoelectron spectroscopy, BET measurements, transmission electron microscopy and optical tools such as UV-visible and photoluminescence spectroscopy.

2. Materials and methods

2.1.Catalyst preparation.

Materials were prepared by means of a microemulsion preparation method with the help of *n*-heptane (Scharlau) as organic media, Triton X-100 (Aldrich) and hexanol as surfactant and cosurfactant, respectively. The titania reference was obtained as a first step using a water in oil microemulsion and titanium tetraisopropoxide (Aldrich) as precursor. In all composite samples the corresponding metal salts; cerium (III) nitrate (Alfa Aesar), bismuth carbonite ($\text{Bi}_2\text{O}_2\text{CO}_3$; Aldrich) and copper(II) nitrate (Aldrich), for $\text{CeO}_2\text{-TiO}_2$, $\text{Bi}_2\text{O}_3\text{-TiO}_2$ and CuO-TiO_2 , respectively, were introduced in the aqueous phase of a microemulsión.^{26,39} The pH of the solution was fixed with nitric acid (2.5 for Bi and 6 for Ce and Cu) under stirring for 30 min. Next, the quantity of tetramethylammonium-hydroxide (TMAH) for Cu and Ce or sodium carbonate for Bi to obtain the corresponding Cu, Ce oxo-hydroxides or Bi carbonate was introduced from the aqueous phase of a similar microemulsion under stirring for ca. 5 min. For nanocomposite samples, a titanium tetraisopropoxide/isopropanol (2:3) solution was subsequently added dropwise on the Ce/Bi/Cu-containing microemulsion. Water/M ($\text{M}=\text{Ti}$, $\text{Ce}+\text{Ti}$, $\text{Bi}+\text{Ti}$, $\text{Cu}+\text{Ti}$) and water/surfactant molar ratios were, respectively, 110 and 18 for all samples. The resulting mixture was stirred for 24 h, centrifuged, and the separated solid precursors rinsed with methanol and dried at 110 °C for 12h. After drying, the solid precursors were subjected to a heating ramp (2 °C min⁻¹) up to 500 °C, maintaining this temperature for 2 h. Sample names are Ti for the titania reference, and xYTi for the composite ones, where x is the molar Ce, Bi or Cu/Ti ratio and Y refers to the corresponding metal.

2.2.Characterization details

Ce, Bi or Cu/Ti composition was analyzed by using inductively coupled plasma and atomic absorption (ICP-AAS; Perkin-Elmer, Optima 3300 DV). Nominal values differ from real ones in less than 3.5 %. X-ray diffraction measurements were performed on Seifert D-500 diffractometer using Ni-filtered Cu Ka radiation and scanning step 0.02°. The BET surface area was measured by N₂ adsorption using a Micromeritics ASAP 2010 system.

UV-visible transmission or diffuse reflectance spectroscopy experiments were performed with a Shimadzu UV2100 apparatus using, for diffuse experiments, BaSO₄ and Teflon as references. Photoluminescence spectra were measured at room temperature on a Fluorescence Spectrophotometer (Perkin Elmer LS50B).

Transmission electron microscopy (HTEM) and X-ray energy dispersive spectra (XEDS) were recorded on a JEOL 2100F TEM/STEM microscope. XEDS analysis was performed in STEM mode, with a probe size ~1 nm, using the INCA x-sight (Oxford Instruments) detector. Specimens were prepared by depositing particles of the samples to be investigated onto a copper grid supporting a perforated carbon film. Deposition was achieved by dipping the grid directly into the powder of the samples to avoid contact with any solvent. The dimensional analysis of the aggregates of particles was performed by fixing the longest longitude as primary axis and defining the orthogonal directions as secondary axes.⁵³

XPS data were recorded on 4 mm × 4 mm pellets with a thickness of ca. 0.5 mm prepared by slightly pressing powdered materials that had been outgassed in the prechamber of the instrument at room temperature at a pressure of $<2 \times 10^{-8}$ Torr. The SPECS spectrometer main chamber, working at a pressure $<10^{-9}$ Torr, was equipped with a PHOIBOS 150 multichannel hemispherical electron analyzer with a dual X-ray

source working with Al K α radiation ($h\nu = 1486.2$ eV) at 120 W, 20 mA using C 1s (284.6 eV) as the energy reference.

2.3.Reaction System

Gas phase photo-oxidation tests were carried out with toluene and using an annular photoreactor. The toluene photooxidation was tested using 0.4 mg cm^{-2} of photocatalyst as a thin layer coating on the internal annulus pyrex tube. The corresponding amount of catalyst was suspended in 1 ml of ethanol, painted on a pyrex tube (cut off at ca. 290 nm) and dried at RT. The reacting mixture ($100 \text{ cm}^3 \text{ min}^{-1}$) was prepared by injecting toluene ($\geq 99\%$; Aldrich) into a wet (ca. 90 % relative humidity, RH) 20 vol. % O₂/N₂ flow before entering the photoreactor, yielding an organic inlet concentration in the range 700 ppmv. After flowing the mixture for ca. 6-8 h (control test) in the dark, the catalyst was irradiated by four fluorescent UV (Sylvania F6WBLT-65; 6W) or Sunlight-type (6W, Sylvania F6W/D) lamps, symmetrically positioned outside the photoreactor. The concentration of reactants and products was analyzed using an on-line gas chromatograph (Agilent GC 6890) equipped with HP-PLOT-Q/HP-Innowax columns (0.5/0.32 mm I.D. x 30 m) and TCD / FID detectors. Measurements were carried out at zero order kinetics with respect to the pollutant concentration, and under stationary conditions, obtained after, at least, 18 h under reaction conditions.⁵³ Carbon balance was achieved in the 96-100 % range for all experiments.

2.4.Analysis of the Quantum Efficiency

The quantum efficiency is defined by the Equation 1. It requires the calculation of the ratio between the number of molecules reacting (reaction rate normalized by the catalytic area) by the number of photons interacting with the catalyst.^{3,48-53}

$$\eta_q = \frac{\langle \text{reaction rate} \rangle (\text{mol m}^{-2}\text{s}^{-1})}{\langle \text{Photon Rate} \rangle (\text{Einstein m}^{-2}\text{s}^{-1})} \times 100 \quad (1)$$

The reaction rate described in Equation A1 requires the measurement of the illuminated surface area and can be calculated as the product of the β Factor and the total superficial area which can be obtained by BET measurements; Equation 2.⁵³

$$A = \beta A_{BET} \quad (2)$$

The estimation of β comes from the calculation of the average effective light path at the sample $\langle e \rangle$.⁵³ This observable measures the average distance or path the light goes through the solid, as mathematically described in Equation 3.

$$\langle e \rangle = \frac{\int_{\lambda} \int_{\Omega} 2/\alpha_{\lambda} I_{\lambda}(x,y,z,\Omega) \underline{\Omega} \cdot \underline{n}_G d\Omega}{\int_{\Omega} I_{\lambda}(x,y,z,\Omega) \underline{\Omega} \cdot \underline{n}_G d\Omega} \quad (3)$$

Where \underline{n}_G is the outwardly directed unit vector normal to the catalytic film. This observable is a function of the lamp spectral properties $I_{\lambda}(x,y,z;\Omega)$, measured at the direction of the solid angle unit vector $\underline{\Omega}$, and the solid absorption coefficient α_{λ} . The calculation is carried out here for 99 % of absorbance ($2/\alpha_{\lambda}$). The average effective light path is calculated as a geometrical average of the values obtained at the (x,y,z) points of the (illuminated) reactor surface according to the mathematical description presented in the Supporting information section.

The β value used in Equation 2 is obtained by the ratio between the effective light path (Equation 3) and the corresponding dimension coming from a model of the solid material estimated with the help of the sample aggregate volume “observed” by light (in turn determined with the help of TEM and porosity measurements –see details of the calculation at the Supporting information section).

To evaluate the photon rate (Equation 1), It is necessary calculate the average superficial rate of photon absorption ($e^{a,s}$), for the catalyst with consideration of the number of charge carrier species involved in the photoreaction (S Factor).

$$\langle \text{Photon Rate} \rangle = e^{a,s}(\underline{x}) S = q_{sup}(\underline{x}) F_{A_s} S \quad (4)$$

In Equation A4, q_{sup} is the radiation flux at each position (x,y,z) of the catalytic film and F_{A_s} is the fraction of light absorbed for the catalytic film. The supporting information present full details of the mathematical procedure to obtain the radiation flux at each position at our reaction system.

The dimensionless S Factor is defined by the Equation 5.

$$S = \sum_i n_i S_i \quad (5)$$

In this equation, i runs over all products of the reaction, S_i and n_i are the fractional selectivity to product i , and the inverse of number of charge carrier species required to obtain the specific i product.

A similar equation (Equation 6) can be used to determinate the apparent quantum efficiency (η_{App}). In this case, according to the IUPAC recommendation,⁴⁷ the denominator of the equation in the radiation flux impinging on the catalytic film ($\langle q \rangle_A$).

$$\eta_q = \frac{\langle \text{reaction rate} \rangle \text{ (mol m}^{-2}\text{s}^{-1})}{\langle q \rangle_A S \text{ (Einstein m}^{-2}\text{s}^{-1})} \times 100 \quad (6)$$

3. Results and Discussion

The XRD patterns presented in Figure 1 are dominated without exception by the diffraction peaks of the anatase polymorph having the $I4_1/amd$ space group. Only at the 30-35 degrees region we observed additional, broad and ill-defined peaks mostly attributable to the brookite phase although in the case of ceria an additional contribution of the fluorite structure ($Fm3m$ space group) may be possible.³⁹ The analysis of the

anatase primary particle size throughout all the samples under study indicates a fairly modest variation in the case of Cu, a decreasing trend in the case of Bi, and a modest increase in the case of Ce (see Table S1 at the Supporting Information). The BET area, also presented in Table S1, behaves accordingly to the anatase primary particle size behavior (i.e. with opposite trend; surface area decreases as particle size increases) though the sample series and differs only modestly from the bare titania reference in the majority of cases. In fact this observable shows a roughly constant value in the three series of catalysts studied expect for the highest Bi loading where a parallel decrease of anatase primary particle size and increase in BET area is observed. The Supporting Information also presents the N₂ adsorption–desorption isotherms and pore size distribution plots for the xCeTi, xBiTi and xCuTi series of samples (Figure S1). All samples exhibited type-IV isotherms with H₂ hysteresis loop, which is the typical behavior of mesoporous material. The samples showed relatively similar pore size distributions with average maximum value between 5 and 10 nm in all cases.

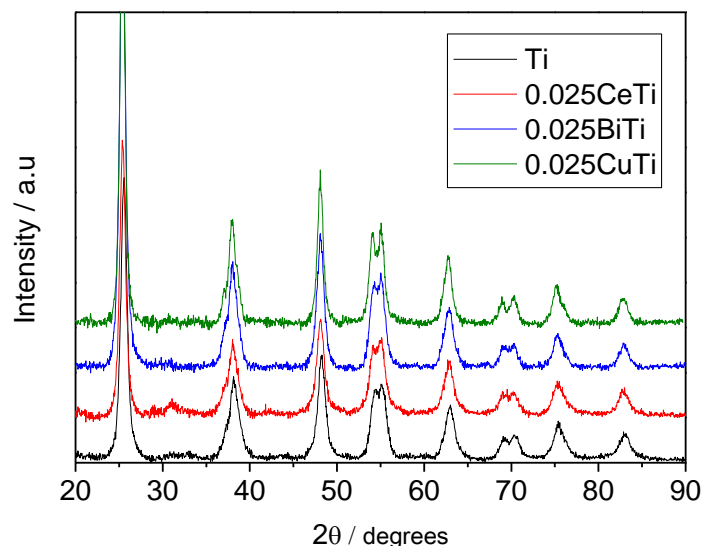


Figure 1. X-ray Diffraction patterns for the titania reference and samples having a 2.5 mol. % surface concentration of alien species.

According to the UV-visible spectra presented in Figure 2 as well as the numerical analysis of anatase band gap (we got a 3.1 eV value considering this material an indirect gap semiconductor –ref. 54) presented in Table S2 at the Supporting information section, rather modest differences can be detected in the band gap of anatase for the small surface loadings of the oxides. The band gap energy decreases for higher loadings, above 1 mol. %. In all samples under study the absence of changes in the anatase diffraction peaks as well as in primary particle size (at least in all cases except the Bi highest loading) strongly indicate that the band gap decreasing trend is mostly an effect of an averaging between the two oxidic species present in the materials and not an effect of a potential doping process of the anatase phase.² In fact, the preparation method forces the sequential, separated precipitation of the two oxide precursors present in the materials. Such fact would minimize the possible presence of alien doping cations in the all oxidic phase or entities. The UV-visible spectra show, at the end part of the characteristic sigmoid curve originated by anatase electronic properties, the presence of localized empty states which contributes to the visible absorption power of the materials and comes from localized and/or electronic transitions of the surface Cu, Bi and Ce ad-species.^{8,11,26,35,39} For our purposes, the main issue is that such optical features increase the light absorption capability of the materials in the visible light region.

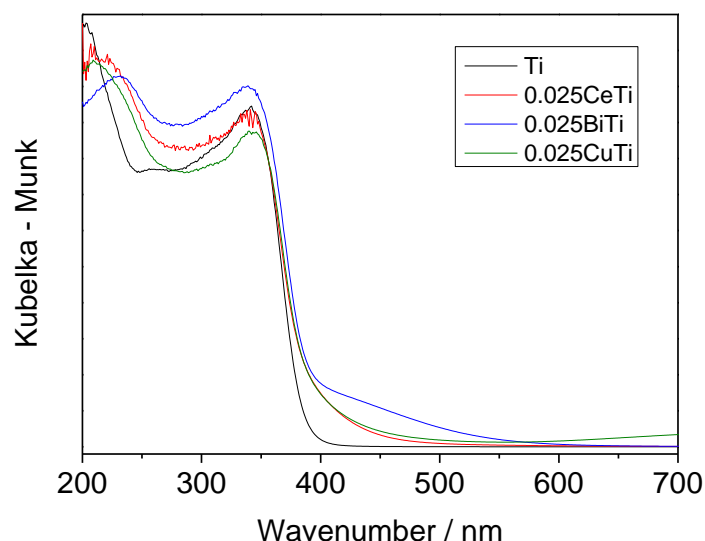


Figure 2. UV-visible spectra for the titania reference and samples having a 2.5 mol. % surface concentration of alien species.

The Cu, Bi and Ce series of samples would thus correspond to materials having an anatase support and surface Cu, Bi and Ce species of different nuclearity and physico-chemical properties. With the exception of the sample having the highest Bi content, we show that the anatase substrate unperturbed (from a physico-chemical point of view). This was further corroborated using TEM. The analysis of morphology and, particularly, the secondary particle size evidences the large similitude among samples (Figure S2). The quantitative analysis of the secondary particles size is presented at the Supporting information Figure S3 and Table S3. Such analysis together with BET measurements suggests a limited effect on morphological parameters of importance (besides primary particle size) in light absorption. We can thus provide evidence that secondary particle size of the main anatase component only differs noticeably from the bare anatase reference in the case of the largest loading of Ce (sample 0.1CeTi). As noted, the constancy of the morphology of the anatase (particularly primary and secondary particle size) is of particularly importance in studying photochemical properties. In our case, it allows the “easy” isolation of catalytic effects directly related

to the surface species present and/or to interface effects produced by interaction with anatase.

High-resolution TEM (Figure 3) with the help of XEDS (Figure 4 and S4) were also used to study the contact between the Cu, Bi, and Ce entities and the dominant anatase phase. The titania component shows platelet-type nanoparticles of ca. 10-15 nm, in agreement with XRD measurements, where smaller, more rounded entities are supported. Representative examples of the alien nanoparticles are marked with arrows in Figure 3. The XEDS study identifies that the smaller particles contain the alien species. Figure 4 compiles the Y:Ti ratios obtained at several (30 per sample) positions of the catalytic solids and provides evidence of the heterogeneity of the surface deposition of the Cu, Bi, and Ce oxide species onto the anatase surface. The comparison of samples having the same molar content suggests that homogeneity and thus dispersion increases moderately in the order $\text{Ce} > \text{Cu} > \text{Bi}$ (see Table S4 at the Supporting Information section for statistical analysis of Y:Ti XEDS atomic ratios). The heterogeneity of the surface deposition process grows, as expected, with the (Cu,Bi,Ce) species content in all systems, being the differences less significant for samples having an alien content below 2.5 mol. %.

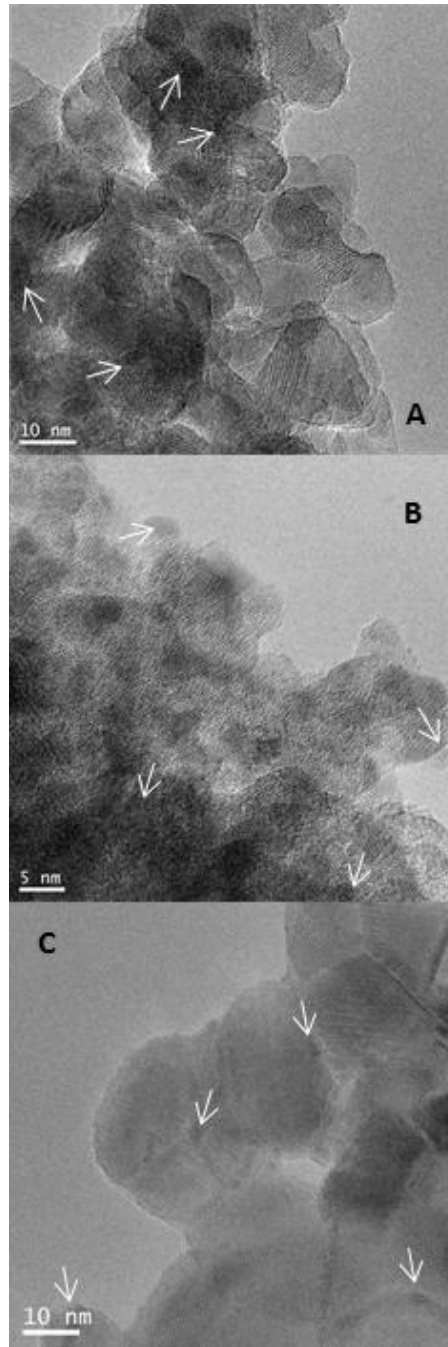


Figure 3. High-resolution TEM images of 0.025CeTi (A); 0.025BiTi (B); and 0.025CuTi (C) samples. Arrows point out the presence of Ce, Bi, and Cu alien species.

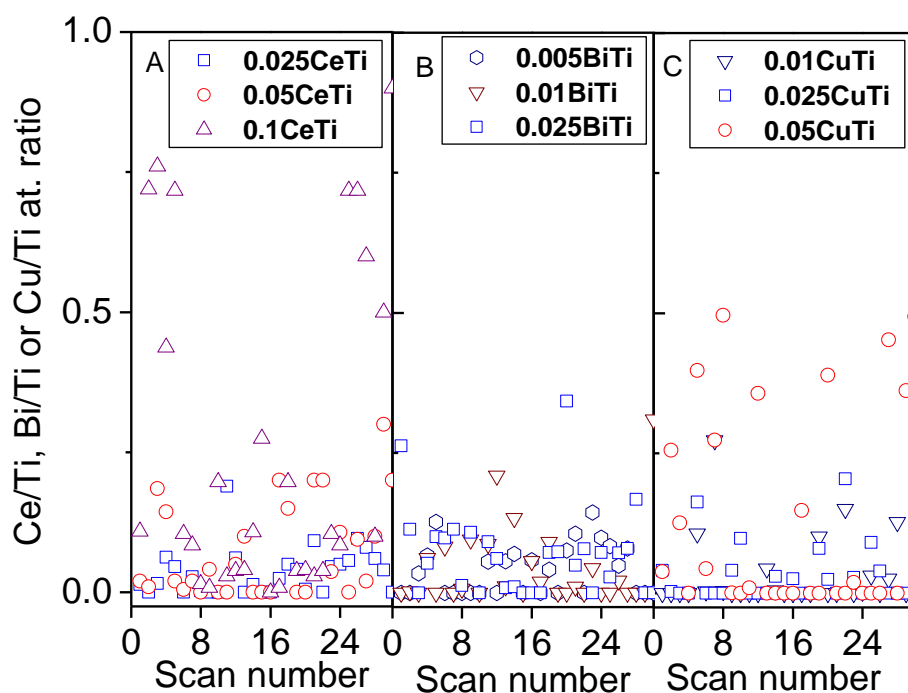


Figure 4. (A) Ce:Ti, (B) Bi:Ti and (C) Cu:Ti atomic ratios as measured by XEDS at several positions of selected samples.

Summarizing the characterization analysis, the only noticeable effects in anatase morphological properties were observed for the highest loading of Bi (mainly variation of primary particle size and subsequent effects in other morphological parameters) and Ce (modifying secondary particle size) series. The Ce modification is however of rather modest magnitude and will have (as shown later) minimal significance in interpreting the behavior of the corresponding Ce-containing series of samples. The basic characterization of the samples additionally evidences the relative similitude of samples for loading at or below 2.5 mol. % in terms not only of anatase support properties but also by the degree of (geometrical) interaction of the alien species and titania and thus in terms of geometrical interface effects.

We measured the reaction rate of toluene photo-degradation: panels A and B of Figure 5 present the surface-normalized reaction rates under UV and sunlight-type illumination, respectively. We previously presented the data for the Bi and Ce series, although the

first was at that time calcined at different temperature.^{27,39} The catalytic results show in all cases the presence of maxima at well defined surface concentration regions. For UV (Fig. 4A) the maximum is reached at relatively low concentrations, 1 mol. % for Cu and Bi, and 2.5 mol. % for Ce series. For Sunlight-type (Fig. 4B) the maximum is attained at higher concentrations for Cu (2.5 mol. %) and Ce (5 mol. %). For Bi and sunlight-type excitation absence of a sample outperforming the anatase reference is noticed. To justify activity here we first attempt to study the materials and particularly the chemical state of the surface species as well as their expected effects in charge handling after UV and visible light excitation.

For such task, we carried out a combined XPS and Photoluminescence study of the materials. Figure 6 provides some illustrative examples of the XPS spectra recorded for the Y cations (Y = Cu, Bi and Ce) deposited onto the anatase surface. A complete collection of XPS spectra for the YTi samples used in this work is presented in Figure S3 at the Supporting Information section. The result of a fitting analysis is also presented in Figure 6 and was carried out with a single (and usual, based in a S-L coupling scheme) assumption of a 3:2 fixed intensity ratio between the Ce3d_{5/2} and Ce3d_{3/2} components for Ce-containing samples.^{39,55,56} Thus, Cu, Bi and Ce chemical contributions to their corresponding 2p, 4f, and 3d spectra were fitted and two oxidation states detected in all cases. The presence of two chemical states having oxidic nature in all our samples can be demonstrated by the binding energy values reported in Tables S6 to S8. Moreover, the co-existence of two oxidic species and a significant contribution of the reduced species for the low loading content range here explored have been found previously in many cases when supporting onto the anatase surface small quantities of Cu,^{8,9,11,57} Bi,^{26,30} and Ce.^{39,58} Specifically, in cases concerning Cu and Ce, this work and previous studies showed the stabilization of Cu¹⁺ (assignment of Cu 2p XPS peaks

by their corresponding binding energies is summarized in Table S6; see refs. 9,11 for assignment) and Ce^{3+} (assignment of all Ce 3d XPS peaks is presented in Table S8; see refs 39,57,58) states at the interface with the anatase component. In the case of Bi, the small quantities of such reduced states (called usually $\text{Bi}^{\delta+}$, with $\delta > 1$; see ref. 26,30 and Table S7 for Bi 4f XPS peak assignment) as well as a different behavior of the reduced state contribution with the Bi surface concentration would suggest that the interaction with anatase favors the presence of the reduced state but it may not be directly or exclusively located at the interface. ²⁶

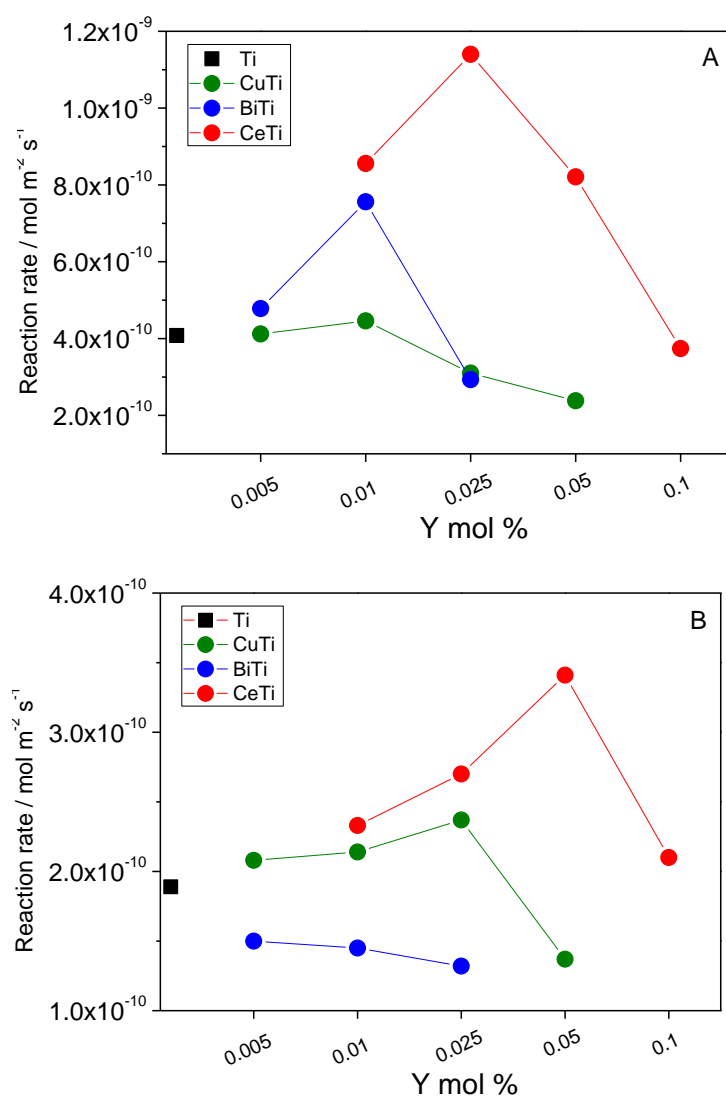


Figure 5. Reaction rate for (A) UV and (B) Sunlight-type illumination conditions.

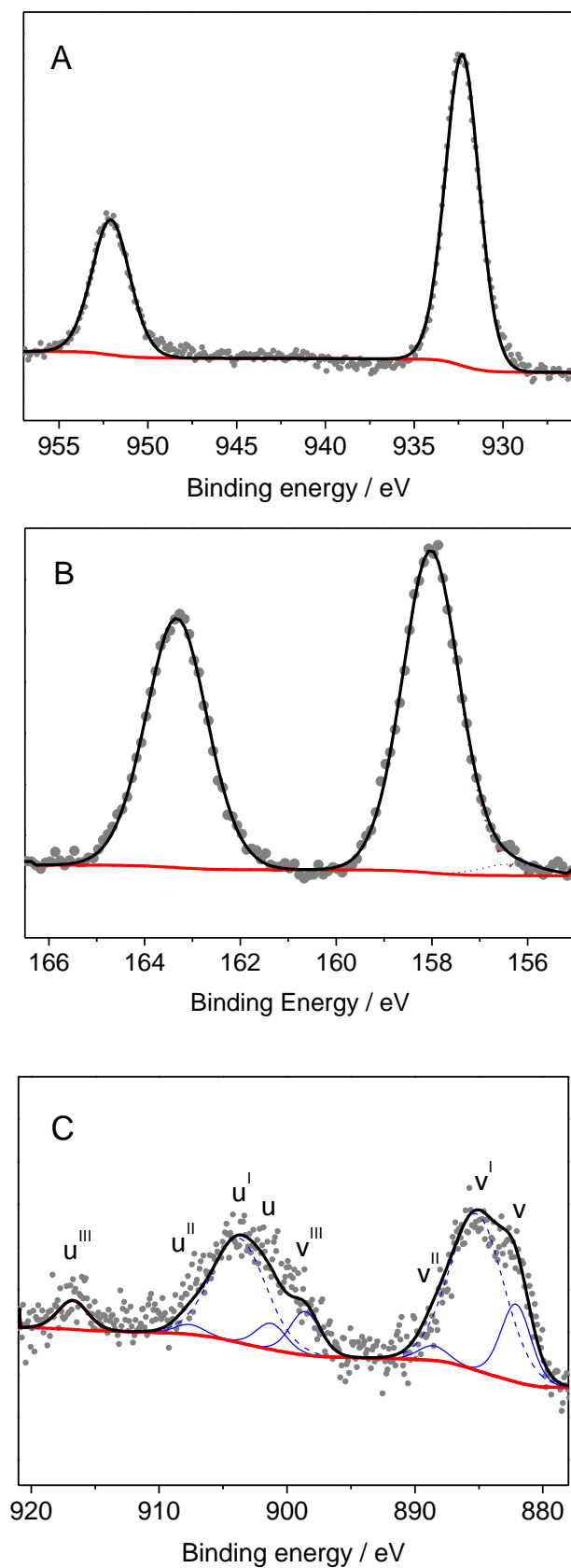


Figure 6. (A) Cu2p, (B) Bi4f and (C) Ce3d XPS spectra for samples having a 1 mol. % surface concentration of alien species. In the case of Ce, Dashed/full line indicates Ce^{3+}/Ce^{4+} contributions.

The contribution of the reduced state (to the total alien atomic population) is presented in Figure 7 using normalized data to take into account the surface area of the materials (a first, rough approximation which will not consider the dispersion of the surface species –a reasonable approximation for the lowest loadings here tested which may have a unit dispersion). The plot displays the area of maximum photocatalytic activity in shadow. Such shadow area corresponds to the maximum contribution of the reduced Y state for UV illumination (left end of the grey box) and the closet, higher loading for Sunlight-type excitation (right end of the grey box). From the study it can be suggested that the surface cations and/or related defects present at the interface with anatase, which do not form well defined oxidic (or semiconductor) phases and thus do not present band-like but just localized electronic states, can be able to capture charge carriers and can provide the basis for leaving holes more freedom (with respect to the bare anatase) to reach the surface of the material and interact with the organic pollutant. As well known, this must have a significant impact in the reaction as it was demonstrated that photo-degradation of toluene in titania-based materials follows a mechanism in which hole-related species play a kinetically determinant role.^{35,39,59–61}

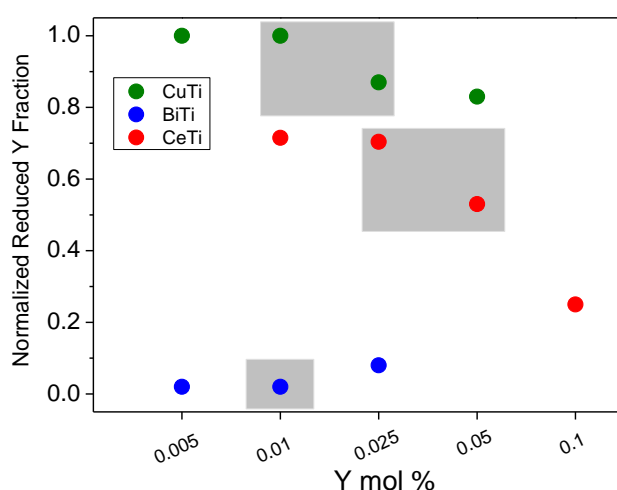


Figure 7. Normalized fraction of the reduced states present at the xYT_i samples. Shaded areas mark values corresponding to the samples having maximum reaction rates.

The hypothesis of charge capture and, more precisely, electron capture by the alien, surface species and the subsequent influence in charge handling is further sustained by photoluminescence experiments. Figure 8 displays results upon UV (385 nm) and Visible (425 nm) illumination. In Figure 8 we compare the experimental results from the samples and the physical mixtures of the two oxides (produced by mixing in a mortar the two oxidic components of each catalyst with the corresponding molar percentages) at the left panels and the intensity of the de-excitation signals in the right panels. The experimental spectra are dominated by a broad feature peaking approximately at 2.5 eV in the case of UV excitation (365 nm). For visible light excitation (425 nm), we observed a decay feature with rather weak peaks at ca. 2.45 and 2.35 eV. As discussed previously, these photoluminescence peaks are characteristic of titania samples and correspond to de-excitation features concerning defects and or localized states as direct (UV-triggered) inter-band de-excitation features are rather weak due to the indirect gap nature of the semiconductor.^{62,63} As the decay profiles among samples are similar and thus no significant differences among samples are expected in de-excitation centers, we focus the discussion on the photoluminescence intensity behavior vs. the cation (Cu, Bi, Ce) content of the catalysts. For the samples having maximum activity, the intensity is always lower than the corresponding to a physical mixture of the components at adequate molar concentration (see right panels at Figure 8). This indicates that the interaction between the Cu, Bi, and Ce oxides and anatase always favors the decrease of the charge recombination after light excitation, irrespective of the light wavelength. Moreover, the intensity behavior through the series clearly correlate with the activity indicating the well-known close relationship between charge handling properties, particularly the effective suppression of recombination, with chemical photo-activity in degradation reactions.^{1,2,5}

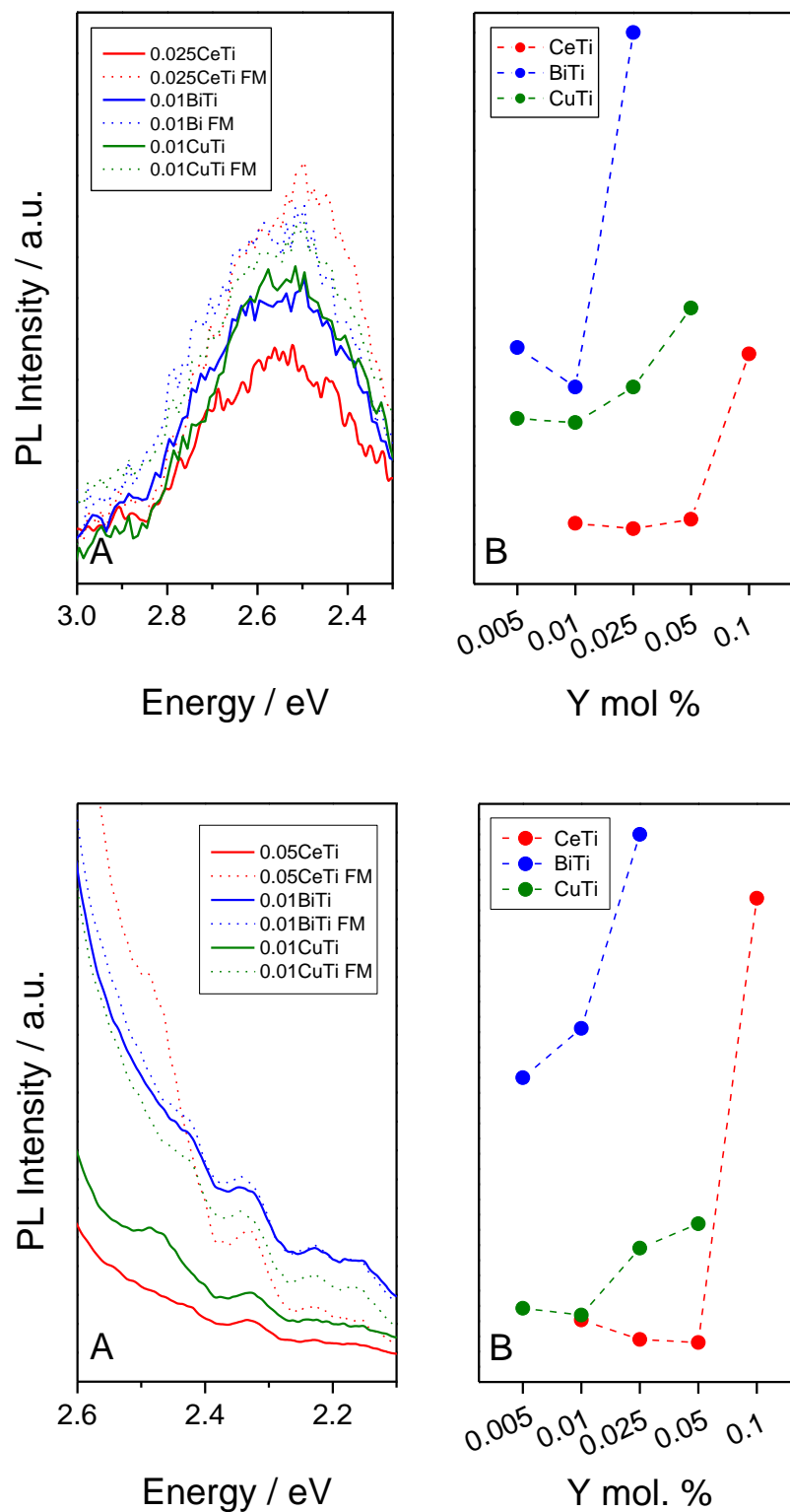


Figure 8. Photoluminescence results obtained upon UV (385 nm; upper panels) and visible (425 nm; lower panels) excitation. (A) panels present photoluminescence spectra for samples presenting maximum reaction rates (full lines) and spectra obtained for a physical mixture of catalyst components (dotted lines). (B) panels present the intensity of the corresponding photoluminescence signals as a function of the surface species concentration.

From the combination of XPS and Photoluminescence results follows that electron trapping by surface species, more properly and according to the literature, by either associated oxygen vacancies (case of Ce, ref. 35) or from a concerted action of anionic defects as well as reduced copper cations (likely the case of Cu; ref. 9) in sharing the extra charge, is providing a route for controlling charge recombination and favor photo-activity. This appears the cases of Cu and Ce. For Bi other effects, such a significant, beneficial and direct effect in the interaction with pollutants of anion vacancies present at the surface (and not exclusively at the interface) of Bi clusters (see, for example, ref. 64), can be likely contributing. Figure 9 shows a graphical representation of the Cu,Bi,Ce oxide-anatase charge handling capabilities and how it provides a route to increase hole species concentration at the surface of the anatase phase, increasing the probability of generating chemistry using this charge carrier species. Upon UV excitation, the alien species always provides a route that facilitates holes reaching the surface of anatase. Upon visible light excitation there are a significant number of charge generation steps but most important related to interface were analyzed in previous publications and are summarized in Figure 9 (2,39). The interface only appears to provide a positive role in charge handling in the case of Ce (39). For Cu, the band alignment between anatase and Cu nano-sized species is expected to separate charge but with potential negative effects by an enhancement of the depletion of hole species at active anatase sites (2). For Bi and as mentioned, at least several charge handling processes may affect the chemical behavior of the samples (2).

In summary, each Cu, Bi, and Ce species handles charge by a different physico-chemical effect as outlined previously in this paragraph, but the general outcome is the critical role of the interface in charge handling and subsequently in the chemistry at the catalyst surface. The interplay of the interface-related effect(s) and the optical

absorption power of the solids would thus define the optimum loading in terms of charge handling properties of the catalytic solids as a function of the surface ad-species concentration. The consistent presence of UV maxima at lower loadings than visible (sunlight-type) ones would indicate that the trade-off between these two effects is marked by a more acute concentration dependence of the absorption capability. The overall result also indicates that chemistry generate by UV excitation is rather important under Sunlight-type illumination.

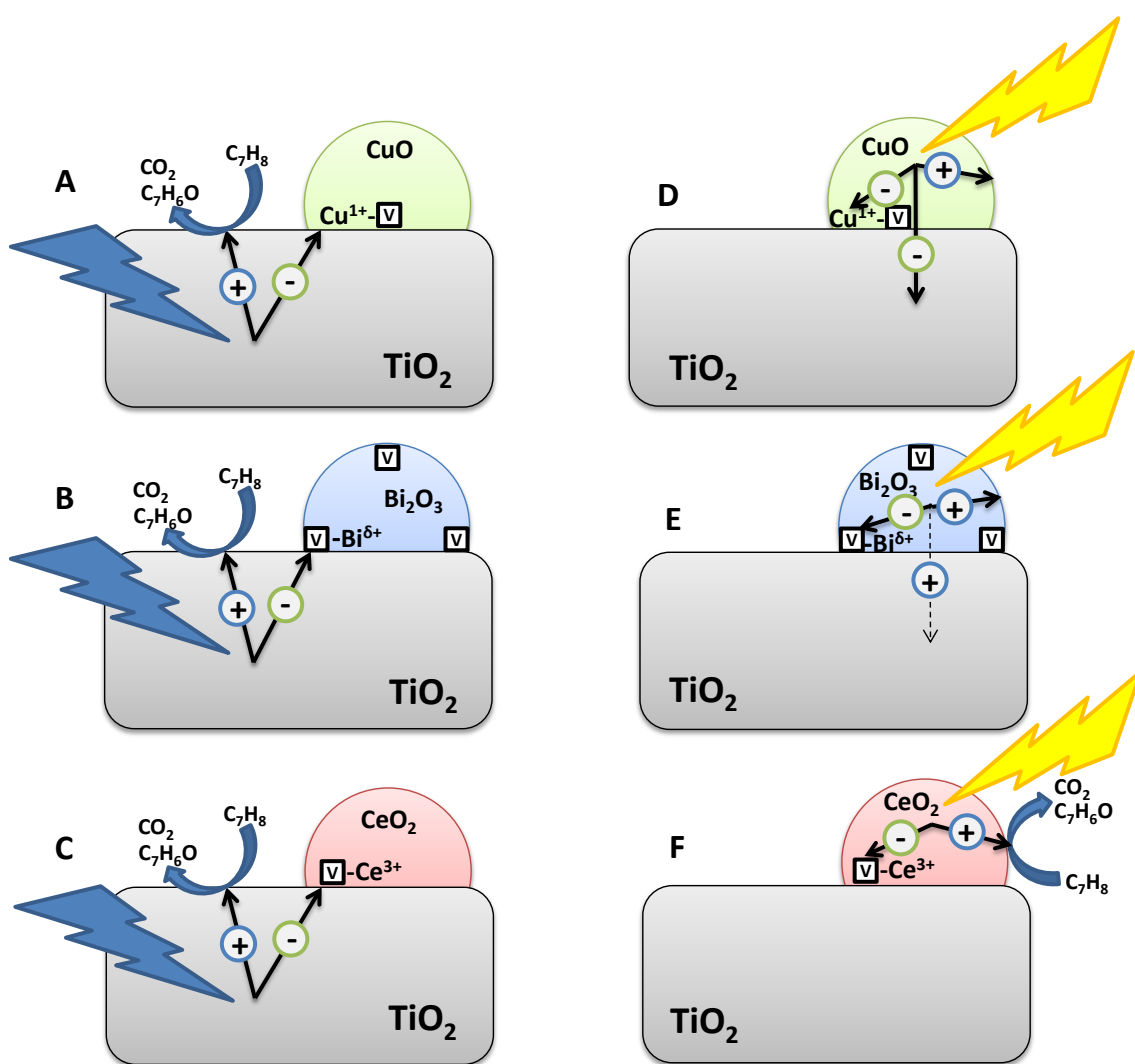


Figure 9. Schematic representation of the interface role in charge handling at xMTi (M=Cu, Bi, Ce) under UV (A,B,C) and Visible (C,D,E) excitation.

The analysis of the quantum efficiency parameter appears, as mentioned in the introduction section, mandatory in order to interpret photo-catalytic activity. In Figures 10 and S8 we presented a study of the quantum efficiency for small surface loadings of the Cu, Bi and Ce containing sample series under UV and Sunlight-type illumination. In the left panel of these figures we presented the normalized (taking the titania reference as unitary value) quantum efficiency with the corresponding reaction rates to highlight potential differences. Central panel compares optical properties as measured by the local rate of photon absorption with the quantum efficiency while the right panel considers the influence of selectivity in the outcome of the efficiency parameter. As described in the experimental section (Equations 1 and 4), the three observables displayed at left axes of Figure 10 control the quantum efficiency value and with this plot we intend to show how they affect the photo-chemical performance in a case where minimal disturbance of the anatase support surface and structural (including morphological) properties takes place.

From Figure 10 we first note that the relative behavior of the reaction rate and quantum efficiency is similar although absolute variations (see the OY scales in the left/right axes) are rather different. The similar trend occurs for UV and Sunlight-type illumination in this specific case, i.e. for samples having a 1 mol. % surface concentration. This is the result of either rather mild variations with respect to titania (Cu series) or of a cancellation effect (Bi and Ce series) between the two physically-independent contributions of the denominator of Equation 1. In the latter case while the local rate of photon absorption presents excess values with respect to the titania reference, the S factor present diminishing values, irrespective of the illumination characteristics. Variations in the denominator of Equation 1 are thus of low magnitude if compared with those concerning the reaction rate (the numerator) in Bi and Ce cases.

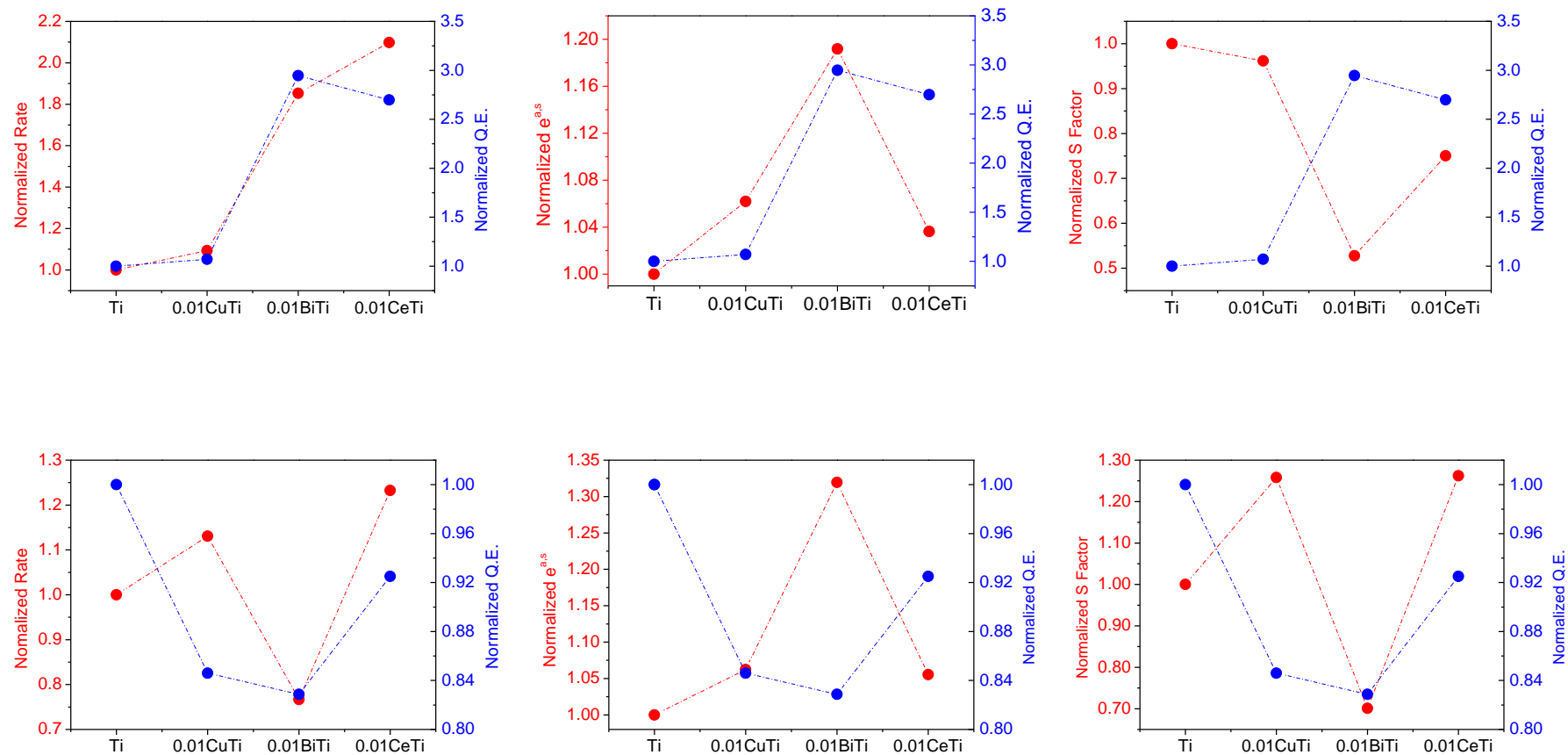


Figure 10. Plot showing the evolution of (normalized) reaction rate, local rate of photon absorption, selectivity factor (left OY axis) and quantum efficiency (right OY axis) observables for samples presenting a concentration of surface species of 1 mol. %. Upper row: UV illumination; Lower row: Sunlight-type illumination.

More importantly, although the interface plays a critical role in charge recombination, the quantum yield behavior (and particularly the difference with the bare titania sample) for samples having a rather minute surface concentration of ad-species (1 mol. %) is also critically determined in the cases of Bi and Ce (i.e. in the cases of optimum efficiency and maximum differences with the titania reference) by effect of the absorption power of the sample and the selectivity of the reaction. If we measured the charge handling effects in photoactivity by the relative decrease of recombination from photoluminescence, the maximum difference among samples is ca. 40/80 % for UV/Sunlight-type (see Figure 9). Such values are comparable with variations of the absorption power (18/32 % for UV/Sunlight-type; see Figure 10) and selectivity (45/30 % for UV/Sunlight-type; see Figure 10). A similar situation in respect to the relative importance of the above mentioned observables is encountered when analyzing the samples having a 2.5 mol. % concentration of the Y (Y=Cu, Bi, Ce) species (Figure S10). Thus in Bi and Ce containing samples and with respect to anatase, we can see that these three physico-chemical observables have the same order of magnitude variation. Although our estimation can be considered just semi-quantitative, it states that catalyst performance depends on the combination of three factors of relatively equal importance. So, in the case where we can safely state that the bare anatase component is a constant in the system (our 1 mol. % loading in xYT_i samples), the three steps including light absorption, the reaching of charge species at the surface of the catalyst as well as their chemical effects as to drive not only activity but also selectivity are of importance to interpret how the titania activity is modified by presence of surface ad-species in relatively small quantities. This is general for the two illumination sources here studied and holds thus some generality in terms of the illumination source.

Another question is how the efficiency of the reaction is maximized. As mentioned, this may not be a simple question when the anatase component is modified but here we showed that maximum efficiency is achieved for samples having relatively low concentration of the surface ad-species. The presence of activity maximum at low loadings, where differences among Cu, Bi and Ce morphological properties at anatase surface are relatively mild according to XRD-TEM-XEDS (Figures 1 and 4; Tables S1 and S4), limits the importance of shadowing effects of the active anatase surface by the alien species, and in turn, the subsequent influence in the activity trends studied. Additionally, the presence of new surface active sites (with respect to bare anatase) can be dismissed as the surface ad-species do not appear to handle charge carrier (hole-related) species directly related to the photochemical process.^{35,39,59–61}

Figure 11 contains the efficiency parameter at various computational levels for titania and xYTi (Y = Cu, Bi, Ce) samples providing maximum efficiency values under, respectively, UV (panel A) and Sunlight-type (panel B) illumination. The plots include calculations using the local net radiation flux (q ; involved in the apparent quantum efficiency calculation) or the local rate of photon absorption ($e^{a,s}$; true quantum efficiency) at the catalyst surface, as well as the influence of considering or not the selectivity of the reaction. It would be important to note that we use the two most common efficiency level of calculation (true or apparent) to show the degree of dependence of the conclusions with the specific level of the calculation. So, when interpreting the active enhancement with respect to the bare titania reference in Figure 11, we can see that for Cu only relatively mild variations are observed; for UV there is essentially no enhancement of the efficiency while for Sunlight-type a small enhancement is visible. A positive effect between the corresponding xYTi (Y=Cu, Bi, Ce-containing) samples and the Ti reference happens only for Bi under UV illumination

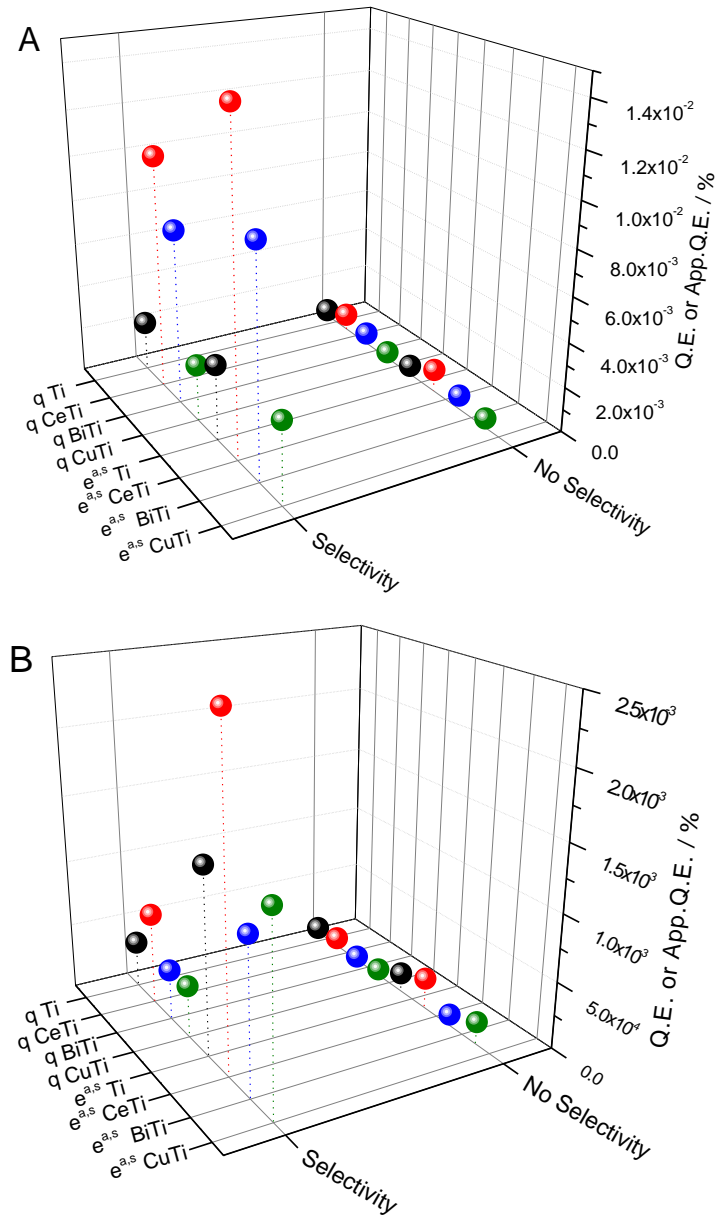


Figure 11. Quantum efficiency values for samples presenting optimum UV (A) and Sunlight-type (B) activity in xYTi series. The titania sample is also included as reference. Values are presented as a function of the computational level used: q; apparent quantum efficiency; e^{a.s}; true quantum efficiency; with/without selectivity.

(enhancement factor of 2.9 using the most accurate calculation level) and Ce upon all illumination conditions (UV factor 4.3; Sunlight-type 1.8) but the magnitude strongly depends of the efficiency level of the calculation. More precisely, there is a constant and important variation while considering or not the selectivity and to a lesser extent of the level of calculation of the optical response of the solid. Such result evidences the

requirement of calculating the efficiency observable at the most stringent level in order to attain meaningful results, even if they are to be utilized in a relative way, using the bare titania as reference.

Using the most accurate calculation of the quantum efficiency (the so called true quantum efficiency), Figure 12 shows the analysis of such observable as a function of its main light-matter and chemical controlling properties (Equations 1 to 5) for UV (upper row) and Sunlight-type (lower row) illumination. As mentioned, we focus on the enhancement with respect to the bare titania reference. Under both UV and Sunlight-type, Cu shows a relatively mild increasing in optical absorption power and relatively small effects of selectivity of different sign (variation of the S factor negative for UV and positive for Sunlight-type). Therefore, in the case of Cu the enhancement in the reaction rate observed is always translated in damped and limited variation(s) of the quantum efficiency. For Bi we observed a significant increase in absorption power with negative effect in efficiency. This is however over- (UV illumination) or partially- (sunlight-type case) balanced by the selectivity factor. The opposite behavior of these two factors but the larger magnitude of the later in both Bi and Ce cases indicates that the quantum efficiency is driven by the differential (with respect to anatase) reaction rate modulated by the selectivity. This clearly shows that not only the number of active charge species reaching the surface (controlled by light absorption and recombination in turn related to the interfacial effects schematically depicted in Figure 9) is critical but their handling for producing different chemical molecules is as important as the reaction rate. Assuming the same active center irrespective of light wavelength (as commonly postulated), this suggests that hot charge carriers, formed under UV with higher probability than under visible excitation, generates preferentially carbon dioxide. Selectivity can be thus somehow related to either differences in the organic matter

attack steps and/or the relaxing mechanism of the active charge species. The elucidation of the situation requires further study.

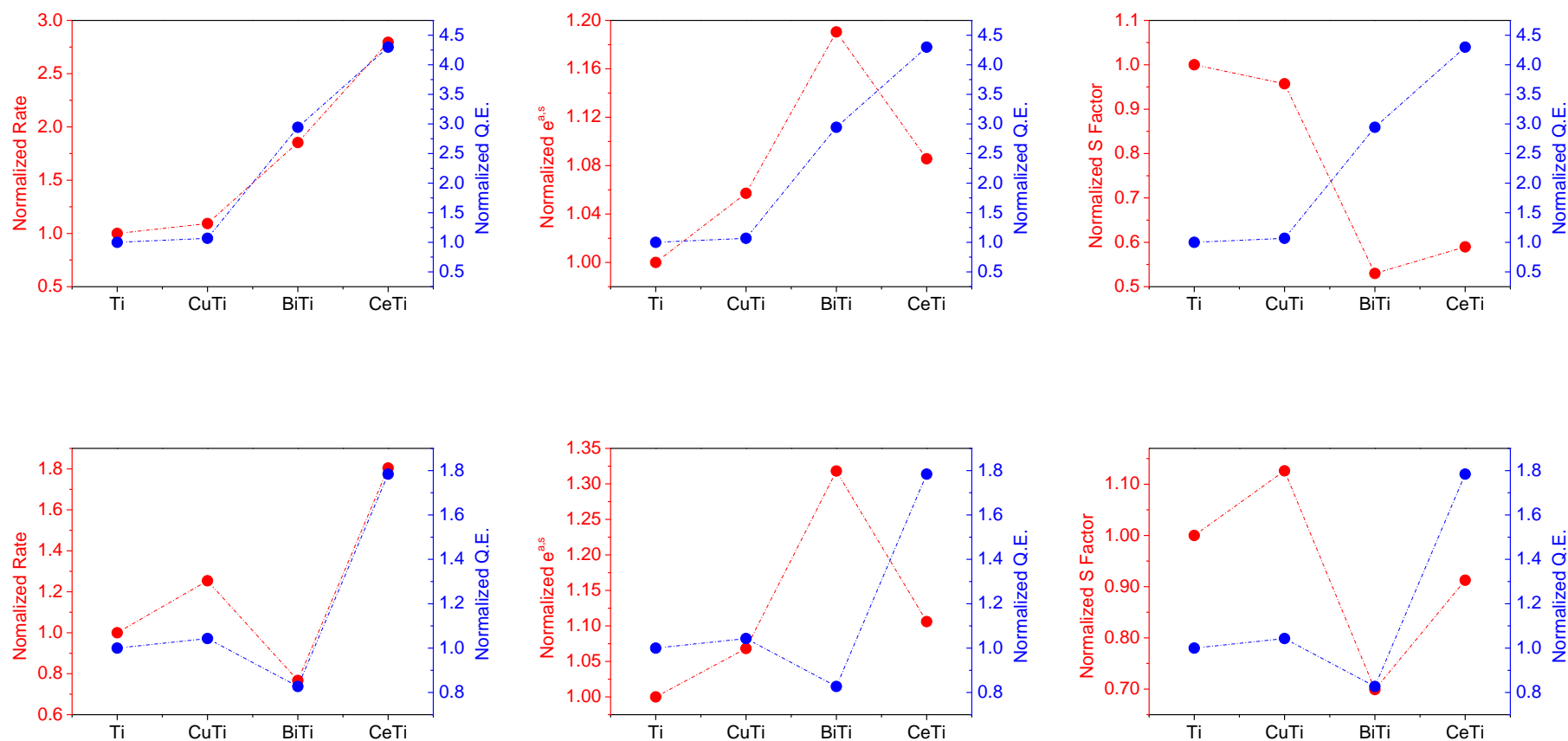


Figure 12. Plot showing the evolution of (normalized) reaction rate, local rate of photon absorption, selectivity factor (left OY axis) and quantum efficiency (right OY axis) observables for samples presenting optimum photo-degradation of toluene. Upper row: UV illumination; Lower row: Sunlight-type illumination.

4. Conclusions

In this work we carried out the surface modification of a high surface area anatase sample by depositing Cu, Bi and Ce oxidic species using a microemulsion method. Samples having a molar concentration of Cu, Bi and Ce surface species in the 0.5 to 10 mol. % range were prepared and subjected to a photocatalytic test for toluene degradation under UV and Sunlight-type illumination. A basic structural and electronic characterization indicate that the anatase component maintains most of its physico-chemical characteristics (in terms of structural, morphological, and electronic properties) at least up to loadings below (Bi) or equal (Cu, Ce) to 2.5 mol. % while moderate changes are observed above such point.

Using this knowledge it was shown that the quantum efficiency in toluene photo-degradation optimization occurs, irrespective of the illumination conditions, with significant influence of all key steps of the photo-chemical reaction, a larger absorption power must be combined with the efficient suppression of recombination, and the adequate handling of reaction selectivity. The similar, quantitative importance of all these aspects in quantum efficiency analysis was proved using limited loadings in order to control anatase modification with respect to the bare system. We also studied how the quantum efficiency observable is maximized within the three (Cu, Bi and Ce) series of samples. First, we showed that such task required the calculation of the true quantum efficiency as simplified formulations may provide rather different answers to the question. We also showed that efficiency optimum occurs for toluene degradation in a way depending of the chemical nature of the surface species. For Cu we always observed relatively mild variations with respect to anatase, damped with respect to those of the reaction rate. Optimum efficiency in toluene photo-degradation was only reached in presence of surface Bi and/or Ce species. In these cases the joint modification of rate

and selectivity with respect to anatase triggers a significant enhancement of the quantum efficiency based in the harmonic interplay of the optoelectronic and chemical characteristics of the active anatase surface. The Cu,Bi,Ce oxide-anatase interface plays a key role in triggering the adequate charge handling of charge carriers affecting optoelectronic properties of the catalytic solids and thus contributing decisively to the optimization of the efficiency parameter for all illumination conditions and series of samples here studied.

Supporting Information

The supporting information section contains results from porosity measurements, as well as TEM, XEDS, and XPS data. It also contains a full description of the mathematical procedures and experimental measurements required to obtain the quantum efficiency observable. It finalizes with the analysis and reporting of average errors of the physic-chemical observables used in the manuscript.

Acknowledgements

Financial support by MINECO (ENE2013-46624-C4-1-R) is gratefully acknowledged. The work of the ICP-CSIC “Unidad de Apoyo” is also thanked.

References

- (1) Hoffmann, M. R.; Martin, S. T.; Choi, W.; Bahnemann, D. W. Environmental Applications of Semiconductor Photocatalysis. *Chem. Rev.* **1995**, 95 (1), 69–96.
- (2) Kubacka, A.; Fernández-García, M.; Colón, G. Advanced Nanoarchitectures for Solar

- Photocatalytic Applications. *Chem. Rev.* **2012**, *112* (3), 1555–1614.
- (3) Alfano, O. M.; Bahnemann, D.; Cassano, A. E.; Dillert, R.; Goslich, R. Photocatalysis in Water Environments Using Artificial and Solar Light. *Catal. Today* **2000**, *58* (2-3), 199–230.
 - (4) Wang, Z.; Liu, Y.; Huang, B.; Dai, Y.; Lou, Z.; Wang, G.; Zhang, X.; Qin, X. Progress on Extending the Light Absorption Spectra of Photocatalysts. *Phys. Chem. Chem. Phys.* **2014**, *16* (7), 2758–2774.
 - (5) Jing, L.; Zhou, W.; Tian, G.; Fu, H. Surface Tuning for Oxide-Based Nanomaterials as Efficient Photocatalysts. *Chem. Soc. Rev.* **2013**, *42* (24), 9509–9549.
 - (6) Colón, G.; Maicu, M.; Hidalgo, M. C.; Navío, J. A. Cu-Doped TiO₂ Systems with Improved Photocatalytic Activity. *Appl. Catal. B Environ.* **2006**, *67* (1-2), 41–51.
 - (7) Kim, T. W.; Ha, H.-W.; Paek, M.-J.; Hyun, S.-H.; Choy, J.-H.; Hwang, S.-J. Unique Phase Transformation Behavior and Visible Light Photocatalytic Activity of Titanium Oxide Hybridized with Copper Oxide. *J. Mater. Chem.* **2010**, *20* (16), 3238–3245.
 - (8) Kubacka, A.; Muñoz-Batista, M. J.; Ferrer, M.; Fernández-García, M. UV and Visible Light Optimization of Anatase TiO₂ Antimicrobial Properties: Surface Deposition of Metal and Oxide (Cu, Zn, Ag) Species. *Appl. Catal. B Environ.* **2013**, *140-141*, 680–690.
 - (9) Sajjad, S.; Leghari, S. A. K.; Zhang, J. Copper Impregnated Ionic Liquid Assisted Mesoporous Titania: Visible Light Photocatalyst. *RSC Adv.* **2013**, *3* (31), 12678–12687.
 - (10) Lin, C.-J.; Yang, W.-T. Ordered Mesostructured Cu-Doped TiO₂ Spheres as Active Visible-Light-Driven Photocatalysts for Degradation of Paracetamol. *Chem. Eng. J.* **2014**, *237*, 131–137.
 - (11) Moniz, S. J. A.; Tang, J. Charge Transfer and Photocatalytic Activity in CuO/TiO₂ Nanoparticle Heterojunctions Synthesised through a Rapid, One-Pot, Microwave Solvothermal Route. *ChemCatChem* **2015**, *7* (11), 1659–1667.
 - (12) Kubacka, A.; Muñoz-Batista, M. J.; Fernández-García, M.; Obregón, S.; Colón, G. Evolution of H₂ Photoproduction with Cu Content on CuO_x-TiO₂ Composite Catalysts Prepared by a Microemulsion Method. *Appl. Catal. B Environ.* **2015**, *163*, 214–222.

- (13) Pham, T.-D.; Lee, B.-K.; Lee, C.-H. The Advanced Removal of Benzene from Aerosols by Photocatalytic Oxidation and Adsorption of Cu-TiO₂/PU under Visible Light Irradiation. *Appl. Catal. B Environ.* **2016**, *182*, 172–183.
- (14) Lei, M.; Wang, N.; Zhu, L.; Zhou, Q.; Nie, G.; Tang, H. Photocatalytic Reductive Degradation of Polybrominated Diphenyl Ethers on CuO/TiO₂ Nanocomposites: A Mechanism Based on the Switching of Photocatalytic Reduction Potential Being Controlled by the Valence State of Copper. *Appl. Catal. B Environ.* **2016**, *182*, 414–423.
- (15) Lee, S. S.; Bai, H.; Liu, Z.; Sun, D. D. Novel-Structured Electrospun TiO₂/CuO Composite Nanofibers for High Efficient Photocatalytic Cogeneration of Clean Water and Energy from Dye Wastewater. *Water Res.* **2013**, *47* (12), 4059–4073.
- (16) Huang, L.; Peng, F.; Wang, H.; Yu, H.; Li, Z. Preparation and Characterization of Cu₂O/TiO₂ Nano–nano Heterostructure Photocatalysts. *Catal. Commun.* **2009**, *10* (14), 1839–1843.
- (17) Sreekantan, S.; Lai, C. W.; Mohd Zaki, S. The Influence of Lead Concentration on Photocatalytic Reduction of Pb(II) Ions Assisted by Cu-TiO₂ Nanotubes. *Int. J. Photoenergy* **2014**, *2014*, 1–7.
- (18) Xu, J.; Ao, Y.; Fu, D.; Yuan, C. Synthesis of Bi₂O₃–TiO₂ Composite Film with High-Photocatalytic Activity under Sunlight Irradiation. *Appl. Surf. Sci.* **2008**, *255* (5), 2365–2369.
- (19) Jing, L.; Wang, J.; Qu, Y.; Luan, Y. Effects of Surface-Modification with Bi₂O₃ on the Thermal Stability and Photoinduced Charge Property of Nanocrystalline Anatase TiO₂ and Its Enhanced Photocatalytic Activity. *Appl. Surf. Sci.* **2009**, *256* (3), 657–663.
- (20) Shmaila, S.; Sajjad, A. K. L.; Chen, F.; Zhang, J. Study on Highly Visible Light Active Bi₂O₃ Loaded Ordered Mesoporous Titania. *Appl. Catal. B Environ.* **2010**, *94* (3–4), 272–280.
- (21) Hou, J.; Yang, C.; Wang, Z.; Jiao, S.; Zhu, H. Bi₂O₃ Quantum Dots Decorated Anatase TiO₂ Nanocrystals with Exposed {001} Facets on Graphene Sheets for Enhanced Visible-Light Photocatalytic Performance. *Appl. Catal. B Environ.* **2013**, *129*, 333–341.

- (22) Huo, Y.; Chen, X.; Zhang, J.; Pan, G.; Jia, J.; Li, H. Ordered Macroporous Bi₂O₃/TiO₂ Film Coated on a Rotating Disk with Enhanced Photocatalytic Activity under Visible Irradiation. *Appl. Catal. B Environ.* **2014**, *148-149*, 550–556.
- (23) Bian, Z.; Zhu, J.; Wang, S.; Cao, Y.; Qian, X.; Li, H. Self-Assembly of Active Bi₂O₃/TiO₂ Visible Photocatalyst with Ordered Mesoporous Structure and Highly Crystallized Anatase. *J. Phys. Chem. C* **2008**, *112* (16), 6258–6262.
- (24) Zhu, J.; Wang, S.; Wang, J.; Zhang, D.; Li, H. Highly Active and Durable Bi₂O₃/TiO₂ Visible Photocatalyst in Flower-like Spheres with Surface-Enriched Bi₂O₃ Quantum Dots. *Appl. Catal. B Environ.* **2011**, *102* (1-2), 120–125.
- (25) Su, K.; Ai, Z.; Zhang, L. Efficient Visible Light-Driven Photocatalytic Degradation of Pentachlorophenol with Bi₂O₃/TiO₂-X. *J. Phys. Chem. C* **2012**, *116* (32), 17118–17123.
- (26) Yang, J.; Wang, X.; Dai, J.; Li, J. Efficient Visible-Light-Driven Photocatalytic Degradation with Bi₂O₃ Coupling Silica Doped TiO₂. *Ind. Eng. Chem. Res.* **2014**, *53* (32), 12575–12586.
- (27) Gómez-Cerezo, M. N.; Muñoz-Batista, M. J.; Tudela, D.; Fernández-García, M.; Kubacka, A. Composite Bi₂O₃-TiO₂ Catalysts for Toluene Photo-Degradation: Ultraviolet and Visible Light Performances. *Appl. Catal. B Environ.* **2014**, *156-157*, 307–313.
- (28) Liu, Y.; Zhao, Q.; Li, X.; Shi, Y.; Li, T. Vacuum-Assisted Impregnation Derived α -Bi₂O₃/TiO₂ Nanotube Arrays with Enhanced Photoelectrochemical Activity. *Mater. Lett.* **2015**, *158*, 104–107.
- (29) Chen, C.; Cao, S.; Long, H.; Qian, G.; Tsang, Y.; Gong, L.; Yu, W.; Xiao, Y. Highly Efficient Photocatalytic Performance of Graphene oxide/TiO₂-Bi₂O₃ Hybrid Coating for Organic Dyes and NO Gas. *J. Mater. Sci. Mater. Electron.* **2015**, *26* (6), 3385–3391.
- (30) Li, D.; Zhang, Y.; Zhang, Y.; Zhou, X.; Guo, S. Fabrication of Bidirectionally Doped β -Bi₂O₃/TiO₂-NTs with Enhanced Photocatalysis under Visible Light Irradiation. *J. Hazard. Mater.* **2013**, *258-259*, 42–49.

- (31) Pavasupree, S.; Suzuki, Y.; Pivsa-Art, S.; Yoshikawa, S. Preparation and Characterization of Mesoporous TiO₂–CeO₂ Nanopowders Respond to Visible Wavelength. *J. Solid State Chem.* **2005**, *178* (1), 128–134.
- (32) Li, G.; Zhang, D.; Yu, J. C. Thermally Stable Ordered Mesoporous CeO₂/TiO₂ Visible-Light Photocatalysts. *Phys. Chem. Chem. Phys.* **2009**, *11* (19), 3775–3782.
- (33) Guzmán, C.; del Ángel, G.; Gómez, R.; Galindo-Hernández, F.; Ángeles-Chavez, C. Degradation of the Herbicide 2,4-Dichlorophenoxyacetic Acid over Au/TiO₂–CeO₂ Photocatalysts: Effect of the CeO₂ Content on the Photoactivity. *Catal. Today* **2011**, *166* (1), 146–151.
- (34) Liu, H.; Wang, M.; Wang, Y.; Liang, Y.; Cao, W.; Su, Y. Ionic Liquid-Templated Synthesis of Mesoporous CeO₂–TiO₂ Nanoparticles and Their Enhanced Photocatalytic Activities under UV or Visible Light. *J. Photochem. Photobiol. A Chem.* **2011**, *223* (2–3), 157–164.
- (35) Muñoz-Batista, M. J.; Kubacka, A.; Gómez-Cerezo, M. N.; Tudela, D.; Fernández-García, M. Sunlight-Driven Toluene Photo-Elimination Using CeO₂-TiO₂ Composite Systems: A Kinetic Study. *Appl. Catal. B Environ.* **2013**, *140-141*, 626–635.
- (36) Wang, Y.; Li, B.; Zhang, C.; Cui, L.; Kang, S.; Li, X.; Zhou, L. Ordered Mesoporous CeO₂-TiO₂ Composites: Highly Efficient Photocatalysts for the Reduction of CO₂ with H₂O under Simulated Solar Irradiation. *Appl. Catal. B Environ.* **2013**, *130-131*, 277–284.
- (37) Liu, Y.; Fang, P.; Cheng, Y.; Gao, Y.; Chen, F.; Liu, Z.; Dai, Y. Study on Enhanced Photocatalytic Performance of Cerium Doped TiO₂-Based Nanosheets. *Chem. Eng. J.* **2013**, *219*, 478–485.
- (38) Karunakaran, C.; Gomathisankar, P. Solvothermal Synthesis of CeO₂–TiO₂ Nanocomposite for Visible Light Photocatalytic Detoxification of Cyanide. *ACS Sustain. Chem. Eng.* **2013**, *1* (12), 1555–1563.
- (39) Muñoz-Batista, M. J.; Gómez-Cerezo, M. N.; Kubacka, A.; Tudela, D.; Fernández-García, M. Role of Interface Contact in CeO₂-TiO₂ Photocatalytic Composite Materials.

- ACS Catal.* **2014**, *4* (1), 63–72.
- (40) Muñoz-Batista, M. J.; Ferrer, M.; Fernández-García, M.; Kubacka, A. Abatement of Organics and Escherichia Coli Using CeO₂-TiO₂ Composite Oxides: Ultraviolet and Visible Light Performances. *Appl. Catal. B Environ.* **2014**, *154-155*, 350–359.
 - (41) Sun, X.; Li, C.; Ruan, L.; Peng, Z.; Zhang, J.; Zhao, J.; Li, Y. Ce-Doped SiO₂@TiO₂ Nanocomposite as an Effective Visible Light Photocatalyst. *J. Alloys Compd.* **2014**, *585*, 800–804.
 - (42) Li, Z.; Sheng, J.; Zhang, Y.; Li, X.; Xu, Y. Role of CeO₂ as Oxygen Promoter in the Accelerated Photocatalytic Degradation of Phenol over Rutile TiO₂. *Appl. Catal. B Environ.* **2015**, *166-167*, 313–319.
 - (43) Verma, R.; Samdarshi, S. K.; Singh, J. Hexagonal Ceria Located at the Interface of Anatase/Rutile TiO₂ Superstructure Optimized for High Activity under Combined UV and Visible-Light Irradiation. *J. Phys. Chem. C* **2015**, *119* (42), 23899–23909.
 - (44) Zeng, M.; Li, Y.; Mao, M.; Bai, J.; Ren, L.; Zhao, X. Synergetic Effect between Photocatalysis on TiO₂ and Thermocatalysis on CeO₂ for Gas-Phase Oxidation of Benzene on TiO₂/CeO₂ Nanocomposites. *ACS Catal.* **2015**, *5*, 3278–3286.
 - (45) Štengl, V.; Bakardjieva, S.; Murafa, N. Preparation and Photocatalytic Activity of Rare Earth Doped TiO₂ Nanoparticles. *Mater. Chem. Phys.* **2009**, *114* (1), 217–226.
 - (46) Wang, Y.; Zhao, J.; Wang, T.; Li, Y.; Li, X.; Yin, J.; Wang, C. CO₂ Photoreduction with H₂O Vapor on Highly Dispersed CeO₂/TiO₂ Catalysts: Surface Species and Their Reactivity. *J. Catal.* **2016**, *337*, 293–302.
 - (47) Braslavsky, S. E.; Braun, A. M.; Cassano, A. E.; Emeline, A. V.; Litter, M. I.; Palmisano, L.; Parmon, V. N.; Serpone, N. Glossary of Terms Used in Photocatalysis and Radiation Catalysis (IUPAC Recommendations 2011). *Pure Appl. Chem.* **2011**, *83* (4), 931–1014.
 - (48) Serpone, N. Relative Photonic Efficiencies and Quantum Yields in Heterogeneous

- Photocatalysis. *J. Photochem. Photobiol. A Chem.* **1997**, *104* (1-3), 1–12.
- (49) Li Puma, G.; Brucato, A. Dimensionless Analysis of Slurry Photocatalytic Reactors Using Two-Flux and Six-Flux Radiation Absorption–scattering Models. *Catal. Today* **2007**, *122* (1-2), 78–90.
- (50) Palmisano, L.; Augugliaro, V.; Campostrini, R.; Schiavello, M. A Proposal for the Quantitative Assessment of Heterogeneous Photocatalytic Processes. *J. Catal.* **1993**, *143* (1), 149–154.
- (51) Brandi, R. J.; Citroni, M. A.; Alfano, O. M.; Cassano, A. E. Absolute Quantum Yields in Photocatalytic Slurry Reactors. *Chem. Eng. Sci.* **2003**, *58* (3-6), 979–985.
- (52) Ohtani, B. Preparing Articles on Photocatalysis—Beyond the Illusions, Misconceptions, and Speculation. *Chem. Lett.* **2008**, *37* (3), 216–229.
- (53) Muñoz-Batista, M. J.; Kubacka, A.; Hungría, A. B.; Fernández-García, M. Heterogeneous Photocatalysis: Light-Matter Interaction and Chemical Effects in Quantum Efficiency Calculations. *J. Catal.* **2015**, *330*, 154–166.
- (54) Fernández-García, M.; Martínez-Arias, A.; Hanson, J. C.; Rodriguez, J. A. Nanostructured Oxides in Chemistry: Characterization and Properties. *Chem. Rev.* **2004**, *104* (9), 4063–4104.
- (55) Paparazzo, E. On the Curve-Fitting of XPS Ce(3d) Spectra of Cerium Oxides. *Mater. Res. Bull.* **2011**, *46* (2), 323–326.
- (56) Wagner, C. D. *Handbook of X-Ray Photoelectron Spectroscopy: A Reference Book of Standard Data for Use in X-Ray Photoelectron Spectroscopy*; Physical Electronics Division, Perkin-Elmer Corp., 1979.
- (57) Baber, A. E.; Yang, X.; Kim, H. Y.; Mudiyansele, K.; Soldemo, M.; Weissenrieder, J.; Senanayake, S. D.; Al-Mahboob, A.; Sadowski, J. T.; Evans, J.; Rodriguez, J. A.; Liu, P.; Hoffmann, F. M.; Chen, J. G.; Stacchiola, D. J. Stabilization of Catalytically Active Cu + Surface Sites on Titanium-Copper Mixed-Oxide Films. *Angew. Chemie* **2014**, *126* (21), 5440–5444.
- (58) Johnston-Peck, A. C.; Senanayake, S. D.; Plata, J. J.; Kundu, S.; Xu, W.; Barrio, L.;

- Graciani, J.; Sanz, J. F.; Navarro, R. M.; Fierro, J. L. G.; Stach, E. A.; Rodriguez, J. A. Nature of the Mixed-Oxide Interface in Ceria–Titania Catalysts: Clusters, Chains, and Nanoparticles. *J. Phys. Chem. C* **2013**, *117* (28), 14463–14471.
- (59) d’Hennezel, O.; Pichat, P.; Ollis, D. F. Benzene and Toluene Gas-Phase Photocatalytic Degradation over H₂O and HCL Pretreated TiO₂: By-Products and Mechanisms. *J. Photochem. Photobiol. A Chem.* **1998**, *118* (3), 197–204.
- (60) Augugliaro, V.; Coluccia, S.; Loddo, V.; Marchese, L.; Martra, G.; Palmisano, L.; Schiavello, M. Photocatalytic Oxidation of Gaseous Toluene on Anatase TiO₂ Catalyst: Mechanistic Aspects and FT-IR Investigation. *Appl. Catal. B Environ.* **1999**, *20* (1), 15–27.
- (61) Muñoz-Batista, M. J.; Kubacka, A.; Fernández-García, M. Effective Enhancement of TiO₂ Photocatalysis by Sinergistic Interaction of Surface Species: From Promoters to Co-Catalysts. *ACS Catal.* **2014**, *4* (12), 4277–4288.
- (62) Tachikawa, T.; Majima, T. Exploring the Spatial Distribution and Transport Behavior of Charge Carriers in a Single Titania Nanowire. *J. Am. Chem. Soc.* **2009**, *131* (24), 8485–8495.
- (63) Mercado, C.; Seeley, Z.; Bandyopadhyay, A.; Bose, S.; McHale, J. L. Photoluminescence of Dense Nanocrystalline Titanium Dioxide Thin Films: Effect of Doping and Thickness and Relation to Gas Sensing. *ACS Appl. Mater. Interfaces* **2011**, *3* (7), 2281–2288.
- (64) Hameed, A.; Montini, T.; Gombac, V.; Fornasiero, P. Surface Phases and Photocatalytic Activity Correlation of Bi₂O₃/Bi₂O₄-X Nanocomposite. *J. Am. Chem. Soc.* **2008**, *130* (30), 9658–9659.

TOC

